Analysis of the oscillatory liquid metal flow in an alternate MHD generator

J. C. Domínguez-Lozoya[a], H. Perales[b] and S. Cuevas[a]
[a] *Instituto de Energías Renovables, Universidad Nacional Autónoma de México, Apartado Postal 34, Temixco, Morelos, 62580 México.*
[b] *Instituto de Ciencias Marinas y Pesquerías, Universidad Veracruzana Hidalgo 617, Col. Río Jamapa, Boca del Río, Veracruz, 94290, México.*

Received 15 October 2018; accepted 1 November 2018

The zero-mean oscillatory flow of a liquid metal in an alternate magnetohydrodynamic electric generator is explored analytically. The flow, confined in a two-dimensional insulating wall duct under a transverse magnetic field, is driven by an externally imposed oscillatory pressure gradient. The flow behaviour is analyzed in two different regions. First, asymptotic solutions for low and high oscillating frequencies in the uniform magnetic field region far from the magnet edges, are used to explore the phase lag produced by the Lorentz force between the velocity and the axial pressure gradient. In addition, the entrance flow region where the oscillatory fluid motion interacts with the non-uniform magnetic field is studied. A perturbation analysis of the boundary layer flow in this region reveals that non-linear effects lead to the appearance of steady streaming vortices superimposed on the harmonic flow. The influence of these vortices on the performance of the generator is analyzed.

Keywords: MHD generator; liquid metal oscillatory flow; steady streaming; perturbation analysis.

PACS: 47.65.-d; 47.15.Rq; 47.15Cb DOI: https://doi.org/10.31349/RevMexFis.65.239

1. Introduction

In the last decade, the interest on magnetohydrodynamic (MHD) electrical generators has been renewed due to its potential applications as converters of acoustic [1, 2] and ocean wave energy [3, 4]. A MHD generator is a device that converts the kinetic energy of an electrically conducting fluid, for instance a liquid metal, into electrical energy through the interaction with a magnetic field. A common MHD generator consists of a duct with a rectangular cross-section immersed in a static magnetic field that is transverse to a pair of insulating walls. The walls parallel to the applied field are electrical conductors (electrodes). When a conducting fluid flows inside the duct, its motion within the imposed magnetic field induces an electrical current perpendicular to both the fluid motion and the applied field that can be extracted through the electrodes connected to an external load. If the fluid motion is unidirectional, a DC current is induced while, if the fluid moves in oscillatory motion, an AC current is generated. In this way, the kinetic energy of the fluid is converted directly into electrical energy without the need of mechanical parts. DC MHD generators were the first to be developed, particularly at high temperatures using plasma as a working fluid [5]. In the late eighties a proposal was made at Los Alamos National Laboratory to transform acoustic power into electrical power through a liquid metal MHD acoustic transducer [6]. In these devices, the thermoacoustic effect is used to generate an oscillatory motion of a conducting fluid in a duct immersed in an applied transverse magnetic field [2, 7, 8]. Alternate liquid metal MHD generators were later proposed to convert the oscillatory motion of ocean waves into electricity [9–11].

A full evaluation of the performance of liquid metal MHD generators should rely on a detailed analysis of the dynamics of the oscillatory flow interacting with a magnetic field. In contrast with steady MHD duct flows that have been widely studied experimentally and theoretically [12], oscillatory MHD flows have been much less explored [13]. In this paper, we use a two-dimensional model of an MHD generator to investigate analytically the laminar liquid metal flow created by an oscillatory pressure gradient (for instance, produced by either thermoacoustic effect or ocean waves) imposed at the extremes of the generator duct. We analyze the flow in two different regions. First, we consider the region far from the edges of the generator where the magnetic field is uniform. With the aim of understanding the interplay of the imposed pressure gradient and the braking Lorentz force created by the interaction of the induced current with the applied magnetic field, asymptotic solutions are derived in the limits of low and high oscillating frequencies. The second analyzed flow region is where the applied magnetic field is non-uniform, that is, the region where the flow enters or leaves the applied magnetic field. Several studies have addressed the MHD unidirectional flow in this region (see for instance [14, 15]), however, it appears that the oscillatory MHD duct flow in a fringing magnetic field has not been previously considered. Assuming high oscillation frequencies, we pay a particular attention to the behavior of the oscillatory boundary layers immersed in the spatially varying magnetic field. These layers, which are a combination of the Stokes and Hartmann layers, determine the flow dynamics to a large extent. Using a perturbation solution, it is found that non-linear effects give rise to steady streaming vortices in the fringing magnetic field. The effect that these vortices may have on the overall performance of the generator is discussed.

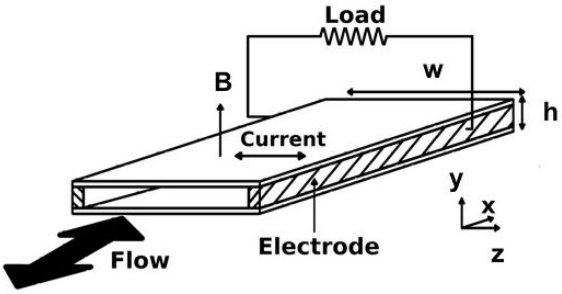

FIGURE 1. Sketch of the MHD alternate generator.

2. Oscillatory flow in an MHD generator

We consider the oscillatory flow of a liquid metal in a duct of rectangular cross-section under a transverse magnetic field. The walls perpendicular to the applied field are electrical insulators, while those parallel to the field are perfect conductors connected to an external load (see Fig. 1). The oscillatory flow is driven by a zero mean, time-periodic pressure gradient imposed at the extremes of the duct.

The system of equations that govern the unsteady flow of an incompressible, electrically conducting viscous fluid in the presence of a magnetic field are the continuity equation, Navier-Stokes equation, Faraday's law of induction, Ampère's law, Gauss's law for the magnetic field and Ohm's law which, respectively, can be conveniently written in the following dimensionless form

$$\nabla \cdot \mathbf{u} = 0, \tag{1}$$

$$\frac{\partial \mathbf{u}}{\partial t} + \frac{R}{R_\omega^2}(\mathbf{u}\cdot\nabla)\mathbf{u} = -\nabla p + \frac{1}{R_\omega}\nabla^2\mathbf{u} + \frac{Ha^2}{R_\omega}\mathbf{j}\times\mathbf{B}, \tag{2}$$

$$\nabla \times \mathbf{E} = -\frac{R_\omega^2}{R}\frac{\partial \mathbf{B}}{\partial t}, \qquad \nabla \times \mathbf{B} = R_m \mathbf{j}, \tag{3}$$

$$\nabla \cdot \mathbf{B} = 0, \qquad \mathbf{j} = \mathbf{E} + \mathbf{u}\times\mathbf{B}, \tag{4}$$

where the flow velocity $\mathbf{u}$, the pressure p, the magnetic field $\mathbf{B}$, the electric field $\mathbf{E}$ and the current density $\mathbf{j}$ are normalized by $U_o = G/\rho\omega$, Gh, B_o, U_oB_o and σU_oB_o, respectively. Here, G and ω are the amplitude and frequency of the imposed oscillatory pressure gradient, ρ and σ are the mass density and the electrical conductivity of the fluid, h is the distance between the walls transverse to the magnetic field, and B_o is the maximum strength of the applied field, respectively. The coordinates (x, y, z) and time t, are normalized by h and $1/\omega$, respectively.

Further, the dimensionless parameters $R_\omega = \omega h^2/\nu$, $R = Gh^3/\rho\nu$, $Ha = B_o h\sqrt{\sigma}\rho\nu$, are the frequency parameter (or oscillation Reynolds number), the amplitude parameter and the Hartmann number, respectively, where ν is the kinematic viscosity. Assuming that the physical and geometrical properties of the system remain unchanged, these dimensionless parameters express, correspondingly, the influence of the oscillation frequency, the amplitude of the pressure gradient, and the magnetic field strength. In turn, $R_m = \mu_0\sigma U_o h$ is the magnetic Reynolds number that gives an estimation of the induced magnetic field compared with the applied field [12], where μ_0 is the magnetic permeability of vacuum.

The oscillatory motion of the fluid inside the magnetic field induces an electric current density in the spanwise (z) direction. The current, in turn, interacts with the applied field originating a braking Lorentz force in the axial x-direction. Usually, in liquid metal MHD flows the low magnetic Reynolds number approximation holds, which means that the magnetic field induced by the fluid motion is much smaller than the applied field and can be neglected [12]. Hence, the magnetic field is uncoupled from the fluid motion and governed by the magnetostatic equations.

3. Flow in the uniform magnetic field region

We now assume that the aspect ratio of the generator is very large, that is, $w/h >> 1$ (see Fig. 1) so that the conducting walls (electrodes) are located at distant positions $z = \pm z_o$, connected to an external electrical circuit. Under this approximation, we can consider that the oscillatory flow is two-dimensional, confined between the insulating walls transverse to the magnetic field (see Fig. 2). Since the current is induced in the direction perpendicular to the plane of motion, there must exist an electric field, E_z, the value of which depends on the external electrical load. As the magnetic field remains unperturbed, Faraday's law of induction reduces to $\nabla \times \mathbf{E} = 0$ and the electric field becomes potential. In fact, it can be shown that under the present assumptions E_z is spatially constant and it is at most a function of time [16].

We now restrict to the region where the applied field is uniform so that, in dimensionless terms, $\mathbf{B} = \hat{\mathbf{y}}$. In this region the flow is fully developed, therefore, $\mathbf{u} = u(y,t)\,\hat{\mathbf{x}}$ and the Navier-Stokes equation reduces to

$$\frac{\partial u}{\partial t} = -\frac{\partial p}{\partial x} + \frac{1}{R_\omega}\frac{\partial^2 u}{\partial y^2} - \frac{Ha^2}{R_\omega}(E_z + u). \tag{5}$$

We disregard transient solutions and consider that the harmonic axial pressure gradient that drives the flow is given by the real part of $-\partial p/\partial x = e^{it}$. Assuming that the axial velocity component and the electric field are also harmonic functions of time, $u = u_0(y)e^{it}$ and $E_z = -Ke^{it}$, with K

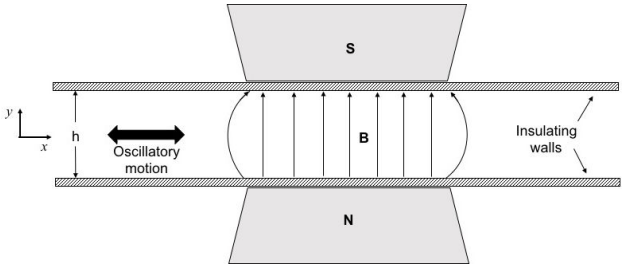

FIGURE 2. Two-dimensional model of the flow in an MHD alternate generator.

a constant known as the load factor [17], a solution to the Eq. (5) that satisfies the no-slip boundary conditions can be found, namely,

$$u(y,t) = U_m e^{it}\lambda\left(\frac{\cosh\lambda - \cosh\lambda y}{\lambda\cosh\lambda - \sinh\lambda}\right), \tag{6}$$

where $\lambda = \sqrt{Ha^2 + iR_\omega}$ and U_m is the dimensionless spatial average of the velocity profile in the cross-section. From this solution it is possible to establish a model of the alternate MHD generator that allows to assess the electrical performance of the device [17].

In the present work the attention is focused in the interplay of inertia and the braking Lorentz force. The explicit form of the velocity profile (6) is, however, not particularly insightful. In order to get a better understanding of the physical behavior of this oscillatory MHD flow, we look for asymptotic solutions in the limits $R_\omega \ll 1$ and $R_\omega \gg 1$, which correspond to the low and high frequency oscillatory motions, respectively.

3.1. Low-frequency solution: $R_\omega \ll 1$

In the low frequency limit it is possible to obtain a regular asymptotic solution in the flow domain [18]. Since we are interested in the limit when R_ω takes very small values, it is convenient to use the rescaled variables $\hat{u} = u/R_\omega$ and $\hat{E}_z = E_z/R_\omega$, so that Eq. (5) becomes

$$R_\omega\frac{\partial\hat{u}}{\partial t} = -\frac{\partial p}{\partial x} + \frac{\partial^2\hat{u}}{\partial y^2} - Ha^2(\hat{E}_z + \hat{u}). \tag{7}$$

Substituting the harmonic pressure gradient and assuming solutions given as the real part of the expressions $\hat{u} = \hat{g}(y)e^{it}$ and $\hat{E}_z = -\hat{K}e^{it}$, an equation for the function $\hat{g}(y)$ is found. We expand this function as a perturbation series on the small parameter R_ω, namely,

$$\hat{g}(y) = \hat{g}_o(y) + R_\omega\hat{g}_1(y) + O(R_\omega^2), \tag{8}$$

and solve the corresponding equations with no-slip boundary conditions at each order on the parameter R_ω. After taking the real part, the final result is

$$\hat{u}(y,t) = \hat{u}_{op}\Bigg\{\left[1 - \frac{\cosh Ha\, y}{\cosh Ha}\right]\cos t + R_\omega\left[\frac{1}{2Ha}\left(y\frac{\sinh Ha\, y}{\cosh Ha} - \tanh Ha\frac{\cosh Ha\, y}{\cosh Ha}\right) + \frac{1}{Ha^2}\left(1 - \frac{\cosh Ha\, y}{\cosh Ha}\right)\right]\sin t\Bigg\} + O(R_\omega^2), \tag{9}$$

where $\hat{u}_{op} = Ha^{-2} + \hat{K}$. At zero-order in R_ω, a quasi-steady Hartmann flow in phase with the pressure gradient oscillation, is obtained. As usual, the profile is flattened as Ha increases [12]. An out of phase contribution is also found at $O(R_\omega)$, but it is modulated by terms of $O(Ha^{-1})$ and $O(Ha^{-2})$ which become negligible the higher the Ha values are. When the Hartmann number is very small, *i.e.* $Ha \to 0$, a purely hydrodynamic flow is recovered

$$\hat{u}(y,t) = \left[\frac{(1-y^2)}{2}\cos t + \frac{R_\omega}{24}(1-y^2)(5-y^2)\sin t\right], \tag{10}$$

which shows an in-phase Poiseuille flow contribution. The phase angle between the pressure gradient and the velocity is given by

$$\theta = \arctan\left[\frac{-R_\omega\left[\frac{1}{2Ha}\left(y\frac{\sinh Hay}{\cosh Ha} - \tanh Ha\frac{\cosh Hay}{\cosh Ha}\right) + \frac{1}{Ha^2}\left(1 - \frac{\cosh Hay}{\cosh Ha}\right)\right]}{\left[1 - \frac{\cosh Hay}{\cosh Ha}\right]}\right] \tag{11}$$

Note that when $Ha \to 0$ viscosity originates a non-zero phase angle, namely, $\theta = -\arctan[R_\omega(5-y^2)/12]$. In turn, when $Ha \to \infty$, the phase angle reduces to zero indicating that the flow is frozen by the strong magnetic field interaction.

3.2. High-frequency solution: $R_\omega \gg 1$

At high frequencies a uniform asymptotic solution for the whole domain does not exist. Therefore, matching asymptotic solutions in the core and the boundary layer has to be sought. For the core, we start from Eq. (5) and introduce the variables $u = g(y)e^{it}$ and $E_z = -Ke^{it}$, assuming that $-\partial p/\partial x = e^{it}$. Hence, we get the equation

$$ig - 1 = \frac{1}{R_\omega}\left[\frac{d^2g}{dy^2} - Ha^2(g-K)\right]. \tag{12}$$

We now look for a solution $g(y)$ as an expansion in the small parameter R_ω^{-1}, namely,

$$g(y) = g_o(y) + \frac{1}{R_\omega}g_1(y) + O(R_\omega^{-2}). \tag{13}$$

Here, we assume that $Ha^2 = \gamma R_\omega$, where γ is a positive real number. Then in the limit $R_\omega \to \infty$, from Eq. (12) and (13), the first order solution in the core is $g_o = (1+\gamma K)/(\gamma+i) =$

$(1+\gamma K)(\gamma - i)/(\gamma^2+1)$. Therefore, the core velocity field is

$$u_c = \frac{(1+\gamma K)}{(\gamma^2+1)}(\gamma\cos t + \sin t) + O(R_\omega^{-2}). \tag{14}$$

This represents a uniform time-periodic flow that lags behind the imposed pressure gradient according to the value of γ, where the phase angle between the pressure gradient and the core velocity is $\theta_c = -\arctan[1/\gamma]$. For $\gamma \ll 1$, a purely hydrodynamic flow is obtained. In this case, the Lorentz force is negligible and there is a lag of $-\pi/2$ in the motion of the core with respect to the pressure gradient. In turn, if $\gamma = 1$, the Lorentz force is of the same order of magnitude as the inertial acceleration, and the core flow presents a phase difference of $-\pi/4$ with respect to the pressure gradient. When $\gamma \gg 1$, the Lorentz force is dominant, therefore, the phase lag is negligible and the core follows the pressure gradient oscillation.

Let us now consider the boundary layer flow. We introduce the stretched variable $Y = R_\omega^{1/2}(1+y)$ in the bottom boundary layer, hence at the wall, $Y = 0$ and $u(0,t) = 0$. Then Eq. (12) becomes

$$\frac{d^2 g_b}{dY^2} - i g_b + 1 = \gamma(g_b - K). \tag{15}$$

for the corresponding function g_b in the boundary layer. Expressing g_b as a series like (13), the solution of Eq. (15) that satisfies no-slip boundary conditions and that matches with the core flow ($g_b\,|_{Y\gg 1} = (1+\gamma K)/(\gamma^2+1)$) within an error of order $O(R_\omega^{-1})$, leads to the boundary layer flow

$$\begin{aligned} u(Y,t) = {} & \frac{(1+\gamma K)}{(\gamma^2+1)} \\ & \times \Big\{ [\gamma - \exp(-\alpha Y)(\gamma\cos\beta Y - \sin\beta Y)]\cos t \\ & + [1 - \exp(-\alpha Y)(\cos\beta Y + \gamma\sin\beta Y)]\sin t \Big\} \\ & + O(R_\omega^{-2}), \end{aligned} \tag{16}$$

where

$$\left.\begin{matrix}\alpha \\ \beta\end{matrix}\right\} = \left[\frac{\sqrt{\gamma^2+1}\pm\gamma}{2}\right]^{1/2}, \tag{17}$$

The phase angle between the boundary layer and the pressure gradient is given by

$$\theta_b = \arctan\left\{\frac{-[1-\exp(-\alpha Y)(\cos\beta Y + \gamma\sin\beta Y)]}{\gamma - \exp(-\alpha Y)(\gamma\cos\beta Y - \sin\beta Y)}\right\}. \tag{18}$$

Again, in-phase and out-of-phase contributions are obtained in the boundary layer, the structure of which depends on the value of γ. Provided $\gamma \ll 1$, a purely hydrodynamic (Stokes) boundary layer is found [18]. When $\gamma = 1$, a mixture of Stokes and Hartmann layers results. Finally, in the case $\gamma \gg 1$, magnetic forces dominate and a Hartmann layer oscillating in phase with the pressure gradient ($\hat{u} \approx (1/R_\omega)[1 - e^{-\sqrt{\gamma}Y}]\cos t$) is obtained.

An illustrative way of visualizing the phase lag produced by the Lorentz force between the velocity and the pressure gradient is by noticing that these quantities satisfy the parametric equations of an ellipse in the plane u vs. $-\partial p/\partial x$ [19]. If we define $X = -\partial p/\partial x$ and $Y = u$, we get for either the core or the boundary layer flows

$$\left(\frac{a^2}{b^2} + 1\right)X^2 - \frac{2a}{fb^2}XY + \frac{Y^2}{f^2 b^2} = 1, \tag{19}$$

where $f(\gamma) = (1+\gamma K)/(\gamma^2+1)$. For the core flow, $a = \gamma$ and $b = 1$, while for the boundary layer flow, we have $a = \gamma - \exp(-\alpha Y)(\alpha\cos\beta Y - \sin\beta Y)$ and $b = 1 - \exp(-\alpha Y)(\cos\beta Y + \gamma\sin\beta Y$. In Figs. 3, Eq. (19) is plotted during a whole cycle for the case $R_\omega = 30$, $K = 0.8$, and different γ values. Some interesting information can be extracted from these plots, particularly because they clearly compare the velocity amplitude before and after the pressure gradient inversion. In fact, the vertical coordinate axis indicates the precise moment at which the pressure gradient is inverted. In the second and fourth quadrants, the pressure gradient acts in favor of the fluid motion, while in the first and third quadrants it acts against the fluid motion. Figure 3a shows the curves corresponding to the core flow. As it was shown, in the laminar hydrodynamic regime ($\gamma = 0$, *i.e.* $Ha = 0$) the core flow presents a phase difference of $-\pi/2$ with respect to the pressure gradient when $R_\omega \gg 1$, and the corresponding curve is a circle. For increasing values of γ, the curve is distorted and rotated clockwise as a result of stronger magnetic interaction which changes the phase difference between the velocity and the pressure gradient. When the Lorentz force is of the same order of magnitude as the inertial acceleration ($\gamma = 1$), a tilted ellipse is obtained while in the case $\gamma \gg 1$ ($Ha \to \infty$), no phase difference exists between the flow and the pressure gradient, therefore, the curve reduces to a straight line. The corresponding curves for the boundary layer flow are shown in Fig. 3b. Although similar ellipses are formed, note that they are not the same as in the core flow since, in addition to the magnetic interaction, viscosity also affects the phase difference between the velocity and the pressure gradient. In fact, no circle is formed even when $Ha = 0$. However, when $\gamma \gg 1$ ($Ha \to \infty$) a straight line is formed indicating that the phase difference disappears.

4. Flow in the non-uniform magnetic field region

In this section, we address the oscillatory flow of the liquid metal close to the edges of the magnets where the magnetic field is non-uniform. In this region, the transverse magnetic field varies from its maximum strength to zero as the x distance to the edge of the magnet increases. Although the cross-section of the duct does not change, this can be considered as an entrance flow problem due the non-homogeneity of the magnetic field. Forced oscillations produced by the imposed

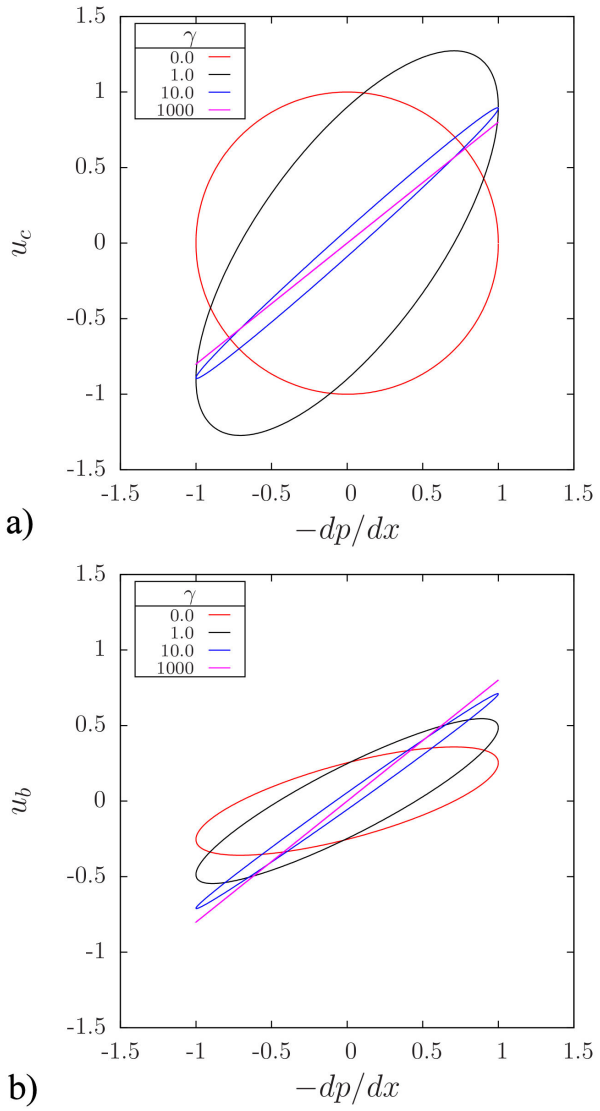

FIGURE 3. (a): The phase-like plane for the core velocity solution for different γ values and $K = 0.8$. (b): The phase-like plane for the boundary layer velocity solution for different γ values, $Y = 0.5$ and $K = 0.8$.

pressure gradient in the outer flow produce an oscillatory flow in the Stokes-Hartmann boundary layer, however, due to the action of viscosity, the flow oscillations in this layer do not average to zero but a net steady flow is produced, known as steady streaming [21, 22]. The steady streaming is induced by the non-linear Reynolds stresses in the boundary layer that appear due to the axial dependence of the streamwise velocity, produced in this case by the existence of the non-uniform field. In hydrodynamic flows, steady streaming appears, for instance, at the entrance of a rigid tube when a zero-mean oscillatory flow is imposed [23] or in the classic problem of oscillating bluff bodies [22,24]. The persistence of the steady streaming beyond the boundary layer is one of the distinctive aspects of this class of oscillatory flows [25]. The action of a uniform transverse magnetic field on the steady streaming produced by an oscillatory laminar boundary layer close to an insulating curved wall was previously studied using a perturbation expansion taking the inverse of the Strouhal number as a small parameter [26]. Following a similar procedure, we explore here the appearance of steady streaming in the boundary layers of the MHD generator promoted by the non-uniformity of the applied transverse magnetic field.

As in Sec. 3, we consider the oscillatory motion of the liquid metal limited by two infinite insulating plane walls at rest under a transverse magnetic field. We are now focused on the region close to the edges of the magnets, so the transverse magnetic field is expressed in the form $\mathbf{B} = B_y(x)\hat{\mathbf{y}}$, where the variation of the field in the axial direction is given in dimensionless form as [15, 27]

$$B_y(x) = \frac{1}{1 + e^{-x/x_0}}. \tag{20}$$

Here x_0 is a positive constant whose magnitude governs the magnetic field gradient. Figure 4 shows the magnetic field distribution for different vales of x_0. We can observe that $B_y \to 0$ as $x \to -\infty$ and $B_y \to 1$ as $x \to \infty$. Although this field is not curl-free, it is a reasonable approximation that take into account the streamwise variation of the magnetic field [15, 27].

We assume that as a result of the imposed pressure gradient, beyond the boundary layer (outer flow) the fluid oscillates irrotationally with a zero-mean in the axial direction so that the corresponding velocity component in dimensionless form can be expressed as the real part of $U(x,t) = U_0(x)e^{it}$. Owing to continuity, the component of the velocity in the perpendicular direction to the wall is $-(y+c)(dU/dx)e^{it}$ where c is a complex constant. The governing equations of the outer flow in dimensionless form are

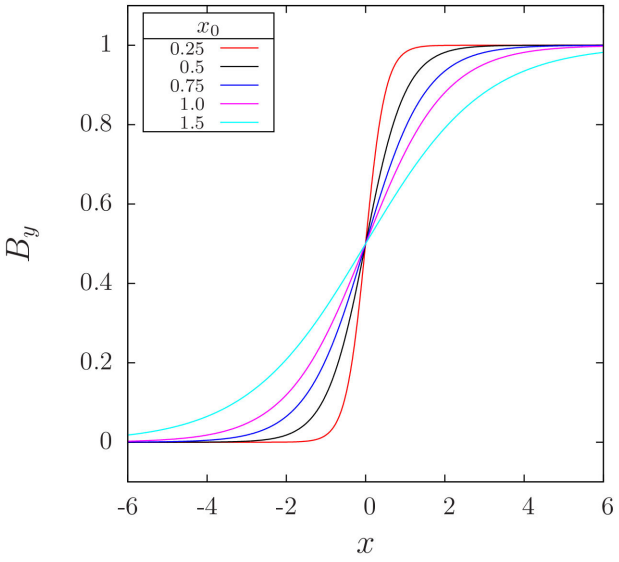

FIGURE 4. Dimensionless applied magnetic field distribution as a function of the axial coordinate x in the magnet edge region for different values of the x_0 parameter.

$$\frac{\partial U}{\partial t} + \epsilon_s U \frac{\partial U}{\partial x} = -N_\omega \frac{\partial p}{\partial x} - N_\omega J_z B_y, \tag{21}$$

$$J_z = E_z + U B_y, \quad \frac{\partial J_z}{\partial z} = 0, \tag{22}$$

where the outer velocity U, the pressure p, the outer current density J_z and the electric field E_z are normalized by U_∞ , $\sigma U_\infty B_0^2 h$, $\sigma U_\infty B_0$ and $U_\infty B_0 h$, respectively. Here U_∞ is the amplitude of the outer flow velocity. Likewise, the coordinates (x, y, z) and time t are normalized by h and $1/\omega$, respectively. Further, the inverse of the Strouhal number, ϵ_s, and the oscillation interaction parameter, N_ω, [26] are given by

$$\epsilon_s = \frac{U_\infty}{\omega h}, \quad N_\omega = \frac{Ha^2}{R_\omega} = \frac{\sigma B_0^2}{\rho \omega}. \tag{23}$$

These dimensionless parameters estimate, respectively, the ratio of the amplitude of the oscillation to the characteristic length h and the ratio of the magnetic to the inertial forces. Equation (21) corresponds to the Euler equation while equations (22) express the Ohm's law and conservation of current in the outer flow. In order to guarantee that boundary-layer separation will not arise, the small amplitude of oscillation approximation is assumed, that is $\epsilon_s \ll 1$.

From Eqs. (21) and (22), the explicit form of the function $U_0(x)$ can be determined at the lowest order in ϵ_s, namely,

$$U_0(x) = \frac{N_\omega (1 + B_y K)}{i + N_\omega B_y^2} \tag{24}$$

where the harmonic variation of the electric field was assumed.

In turn, the inner layer flow is governed by the equations:

$$\frac{\partial u}{\partial x} + \frac{\partial v}{\partial y} = 0 \tag{25}$$

$$\frac{\partial u}{\partial t} + \epsilon_s \left(u \frac{\partial u}{\partial x} + v \frac{\partial u}{\partial y} \right) = -N_\omega \frac{\partial p}{\partial x} + \frac{1}{R_\omega} \frac{\partial^2 u}{\partial y} - N_\omega j_z B_y \tag{26}$$

$$j_z = E_z + u B_y, \quad \frac{\partial j_z}{\partial z} = 0, \tag{27}$$

where U_∞ and $\sigma U_\infty B_0$ have been used to normalize the velocity components in $x-$ and $y-$directions (u and v) and the inner current density, j_z, respectively. In order to ensure the validity of the boundary-layer approximation for the inner flow, it is assumed that $R_\omega \gg 1$. The boundary conditions to be satisfied by the inner flow are

$$u(x, 0, t) = 0, \tag{28}$$

$$v(x, 0, t) = 0, \tag{29}$$

$$u(x, y, t) \longrightarrow U(x, t); \quad \text{as} \quad y \longrightarrow \infty, \tag{30}$$

where (28) and (29) represent the no-slip condition of the velocity components at the wall and (30) is the matching condition for the inner and outer flows.

4.1. First order solution

We now look for a solution of the boundary layer problem as a perturbation expansion in the small parameter ϵ_s. From the incompressible condition, the velocity components are

$$u = \frac{\partial \psi}{\partial y}, \quad v = -\frac{\partial \psi}{\partial x}, \tag{31}$$

where ψ is the stream function that can be expressed in the form

$$\psi(x, y, t) = \psi_0(x, y, t) + \epsilon_s \psi_1(x, y, t) + O(\epsilon_s^2). \tag{32}$$

where the first and second approximations are denoted, respectively, by subindexes 0 and 1. By eliminating the pressure gradient and current densities in Eq. (26) with the substitution of Eqs. (21), (22), (27), and using (31) and (32), we find that ψ_0 satisfies the equation

$$\frac{\partial^2 \psi_0}{\partial t \partial y} - \frac{1}{R_\omega} \frac{\partial^3 \psi_0}{\partial y^3} + N_\omega B_y^2 \frac{\partial \psi_0}{\partial y} = \frac{\partial U}{\partial t} + N_\omega B_y^2 U, \tag{33}$$

with boundary conditions

$$\frac{\partial \psi_0}{\partial y}(x, 0, t) = 0, \tag{34}$$

$$\frac{\partial \psi_0}{\partial x}(x, 0, t) = 0, \tag{35}$$

$$\frac{\partial \psi_0}{\partial y}(x, y, t) \longrightarrow U(x, t); \quad \text{as} \quad y \longrightarrow \infty. \tag{36}$$

Assuming that

$$\psi_0(x, y, t) = U_0(x) \xi_0(x, y) e^{it}, \tag{37}$$

the function ξ_0 satisfies

$$\frac{\partial^3 \xi_0}{\partial y^3} - \frac{\partial \xi_0}{\partial y} \left[i R_\omega + Ha^2 B_y^2 \right] = -(Ha^2 B_y^2 + i R_\omega), \tag{38}$$

with boundary conditions

$$\xi_0(x, 0) = \frac{\partial \xi_0(x, 0)}{\partial y} = 0, \quad \frac{\partial \xi_0(x, y)}{\partial y} \longrightarrow 1 \quad \text{as} \quad y \longrightarrow \infty. \tag{39}$$

The solution of (38) that satisfies conditions (39) is

$$\xi_0(x, y) = y - \frac{1}{\alpha + i\beta}(1 - e^{-(\alpha + i\beta)y}), \tag{40}$$

where

$$\alpha(x) = \left[\frac{\sqrt{Ha^4 B_y^4 + R_\omega^2} + Ha^2 B_y^2}{2} \right]^{\frac{1}{2}},$$

$$\beta(x) = \left[\frac{\sqrt{Ha^4 B_y^4 + R_\omega^2} - Ha^2 B_y^2}{2} \right]^{\frac{1}{2}}.$$

From the solution (40) it is possible to estimate the thickness of the Stokes-Hartmann boundary layer, namely, $\delta \approx 1/[\alpha(x)^2+\beta(x)^2]^{1/2}$. Notice that due to the streamwise variation of the magnetic field, the layer thickness is not uniform in this region. The layer is much thinner where the magnetic field is strong ($B_y \approx 1$). If $Ha^2 \gg R_\omega$, the layer thickness is of the order of the Hartmann layer, namely, $\delta \approx Ha^{-1}$ [12]. Far enough from the magnet edges, say $x < 10x_0$, the magnetic field vanishes so that $Ha = 0$, and the velocity components reduce to

$$u_0 = U_0(x)e^{it}(1 - e^{-(1+i)\eta}),$$
$$v_0 = -\frac{dU_0}{dx}e^{it}\left(\eta - \frac{1}{2}(1-i)\left[1 - e^{-(1+i)\eta}\right]\right),$$

which coincide with the ordinary hydrodynamic limit [21], where $\eta = y\sqrt{R_\omega/2}$. In that region, the layer thickness reduces to that of the Stokes layer, that is $\delta \approx 1/R_\omega^{1/2}$.

4.2. Second order approximation

The equation for the second order approximation ψ_1 to order ϵ has the form

$$\frac{\partial^2\psi_1}{\partial t\partial y} - \frac{1}{R_\omega}\frac{\partial^3\psi_1}{\partial y^3} + N_\omega B_y^2\frac{\partial\psi_1}{\partial y} = U\frac{\partial U}{\partial x} - \frac{\partial\psi_0}{\partial y}\frac{\partial^2\psi_0}{\partial x\partial y} + \frac{\partial\psi_0}{\partial x}\frac{\partial^2\psi_0}{\partial y^2}. \quad (41)$$

Note that the products of the harmonic functions and derivatives on the right-hand side of (41) introduce terms proportional to $\sin 2t$ and $\cos 2t$, as well as steady-state terms. This means that convective non-linear terms give rise to steady state terms that contribute to the steady streaming flow. In order to solve Eq. (41) we assume that

$$\psi_1(x,y,t) = U_0\frac{dU_0}{dx}\left(\xi_{1t}(x,y)e^{2it} + \xi_{1s}(x,y)\right), \quad (42)$$

where the real part of $U_0(x)$ must be taken. The equation satisfied by ξ_{1t} is

$$\frac{\partial^3\xi_{1t}}{\partial y^3} - (Ha^2B_y^2 + 2iR_\omega)\frac{\partial\xi_{1t}}{\partial y} = -\frac{R_\omega}{2}\left[1 - \left(\frac{\partial\xi_0}{\partial y}^2 + \frac{\partial\xi_0}{\partial y}\frac{\partial^2\xi_0}{\partial x\partial y}\frac{U_0(x)}{U_0'(x)}\right) + \xi_0\frac{\partial^2\xi_0}{\partial y^2} + \frac{U_0(x)}{U_0'(x)}\frac{\partial\xi_0}{\partial x}\frac{\partial^2\xi_0}{\partial y^2}\right], \quad (43)$$

with boundary conditions

$$\xi_{1t}(x,0) = \frac{\partial\xi_{1t}}{\partial y}(x,0) = 0 \quad \text{and} \quad \frac{\partial\xi_{1t}}{\partial y} \longrightarrow 0 \quad \text{as} \quad y \longrightarrow \infty. \quad (44)$$

The solution is given in the form

$$\xi_{1t}(x,y) = \frac{R_\omega}{4U_0'(x)}\left[\kappa_{t1}e^{-\lambda y} + \kappa_{t2}e^{-\gamma y} + \kappa_{t3}e^{-2\gamma y} + \kappa_{t4}\right], \quad (45)$$

with $\gamma = \alpha(x) + i\beta(x)$ and $\lambda = \alpha_t(x) + i\beta_t(x)$, where

$$\alpha_t(x) = \left[\frac{\sqrt{Ha^4B_y^4 + 4R_\omega^2} + Ha^2B_y^2}{2}\right]^{\frac{1}{2}},$$

$$\beta_t(x) = \left[\frac{\sqrt{Ha^4B_y^4 + 4R_\omega^2} - Ha^2B_y^2}{2}\right]^{\frac{1}{2}}.$$

The constants κ_{t1}, κ_{t2}, κ_{t3}, and κ_{t4} in (45) are defined in the Appendix.

Solution (45) correctly recovers the hydrodynamic solution [21] when the magnetic field strength tends to zero. Particularly, the contribution to the tangential velocity reduces to

$$\frac{\partial\xi_{1t}(x,y)}{\partial y} = \frac{1}{2}\left[-ie^{-(1+i)\sqrt{2}\eta} + ie^{-(1+i)\eta} - (i-1)\eta e^{-(1+i)}\eta\right]. \quad (46)$$

In turn, the boundary value problem satisfied by the steady state part, ξ_{1s}, is

$$\frac{\partial^3\xi_{1s}}{\partial y^3} - \lambda_s^2\frac{\partial\xi_{1s}}{\partial y} = \frac{R_\omega}{4}\left[2 - 2\frac{\partial\xi_0}{\partial y}\overline{\frac{\partial\xi_0}{\partial y}} + \xi_0\overline{\frac{\partial^2\xi_0}{\partial y^2}} + \overline{\xi_0}\frac{\partial^2\xi_0}{\partial y^2} + \frac{U_0(x)}{U_0'(x)}\left(-\frac{\partial\xi_0}{\partial y}\overline{\frac{\partial^2\xi_0}{\partial x\partial y}} - \overline{\frac{\partial\xi_0}{\partial y}}\frac{\partial^2\xi_0}{\partial x\partial y} + \frac{\partial^2\xi_0}{\partial y^2}\overline{\frac{\partial\xi_0}{\partial x}} + \overline{\frac{\partial^2\xi_0}{\partial y^2}}\frac{\partial\xi_0}{\partial x}\right)\right], \quad (47)$$

$$\xi_{1s} = \xi_{1s}^{'} = 0, \quad \text{at} \quad y = 0, \quad (48)$$

$$\xi_{1s}^{'} \longrightarrow 0, \quad \text{as} \quad y \longrightarrow \infty, \quad (49)$$

where conjugate complex quantities are denoted by an overbar and $\lambda_s = Ha^2B_y(x)$. The solution of equation (47) that satisfies the required boundary conditions is

$$\xi_{1s}(x,y) = \frac{R_\omega}{U_0'(x)\kappa_{s6}}\left(\kappa_{s1}e^{-2\alpha y} + 2\kappa_{s2}e^{-\lambda_s y} - e^{-\alpha y}(\kappa_{s4}e^{i\beta y} + \kappa_{s5}e^{-i\beta y}) + \kappa_{s3}\right), \quad (50)$$

where constants $\kappa_{sj} (j = 1 \text{ to } 6)$ are defined in the appendix. It can be shown that taking the limit of vanishing magnetic field, Eq. (50) and its derivative reduce to the corresponding expressions for the hydrodynamic flow [21, 26].

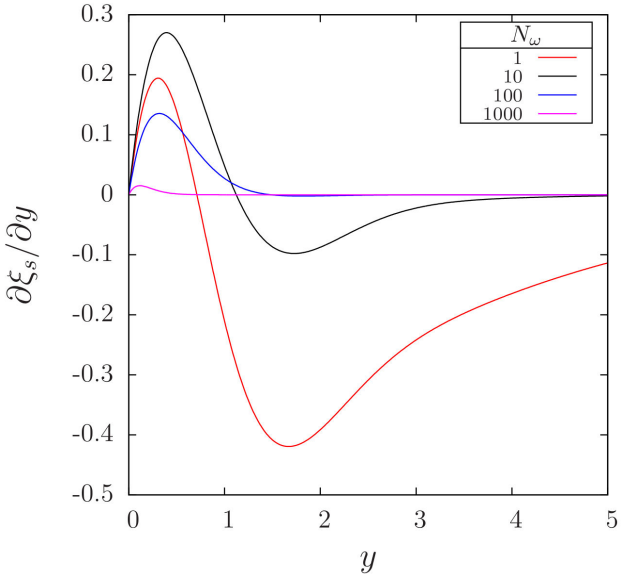

FIGURE 5. $\partial\xi_{1s}/\partial y$ as a function of the y-coordinate for different values of N_ω at a fixed position within the fringing field ($x = 0.5$). $R_\omega = 10$, $K = 0.8$ and $x_0 = 0.5$.

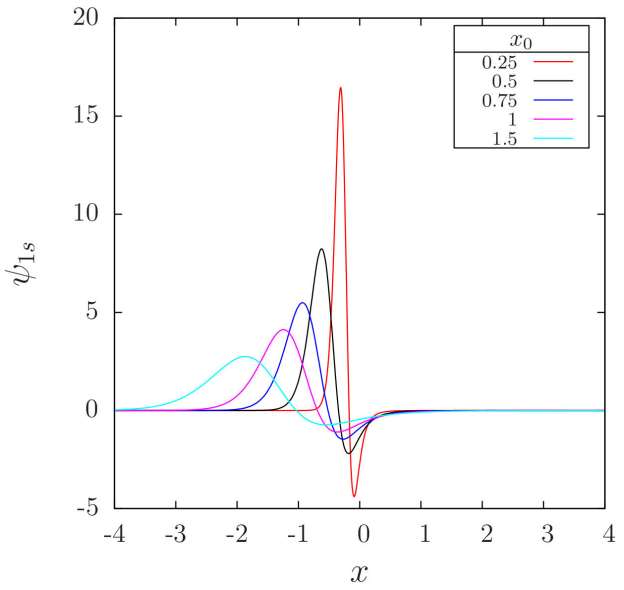

FIGURE 6. Steady part of the stream function, $\psi_{1s}(x, y) = U_0(dU_0/dx)\xi_{1s}$ as a function of the x-coordinate at $y = 1$, for different values of the constant x_0 that modulates the magnetic field gradient. $R_\omega = 10$, $N_\omega = 10$, $K = 0.8$.

In the boundary layer, the second order steady velocity component parallel to the wall is given by

$$u_{1s} = \epsilon_s U_0 \frac{dU_0}{dx}\frac{\partial \xi_{1s}}{\partial y},$$

where $\partial\xi_{1s}/\partial y$ can be obtained from Eq. (50). In the hydrodynamic case (*i.e.* vanishing magnetic field) it results that, as the distance from the wall tends to infinity, u_{1s} does not tend to zero. As a matter of fact, in this case it is not possible to satisfy simultaneously the condition $u_{1s} \to 0$ as $\eta \to \infty$ as

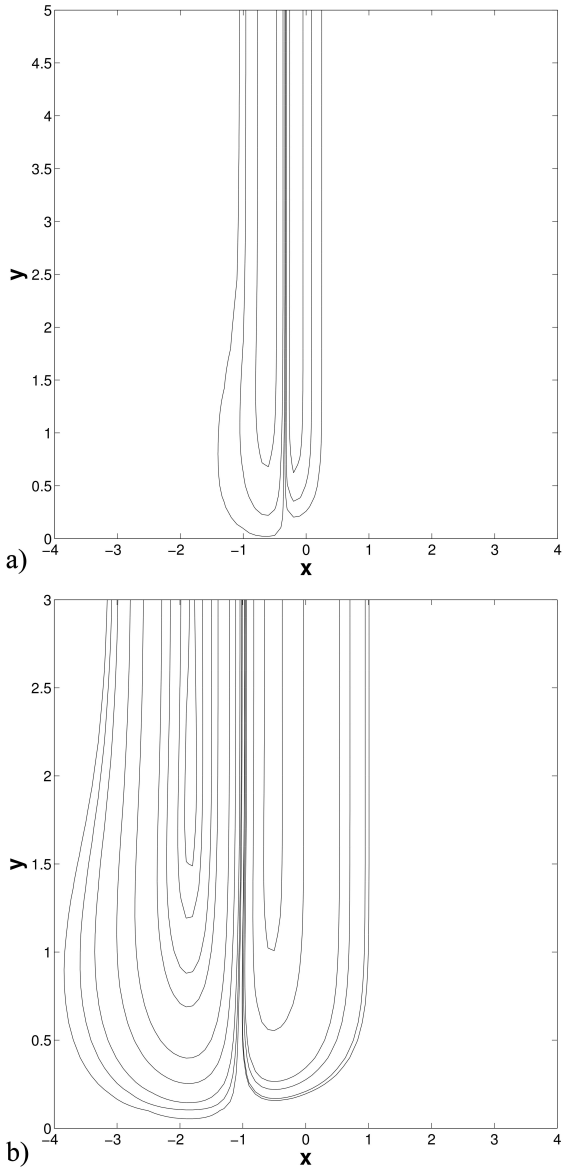

FIGURE 7. Stream lines of the steady streaming flow $\psi_{1s}(x, y) = U_0(dU_0/dx)\xi_{1s}$ in the region of non-uniform magnetic field. $R_\omega = 10$, $N_\omega = 10$ and (a) $x_0 = 0.5$ and (b) $x_0 = 1.5$.

well as the non-slip condition at the wall [21, 25]. Therefore, the condition at infinity must be relaxed, imposing that u_{1s} remains finite as the distance from the wall tends to infinity.

In this way, the steady streaming flow goes beyond the boundary layer, penetrating into the potential flow. The finite velocity at the edge of the boundary layer can be used as the inner boundary condition for the outer flow [25]. Although far form the magnet edges $\partial\xi_{1s}/\partial y$ tends to the hydrodynamic limit as $y \to \infty$, notice that $dU/dx \to 0$ when the magnetic field is negligible. Therefore, the steady streaming disappears in the purely hydrodynamic region. Evidently, dU/dx is also zero in the uniform magnetic field region.

Unlike the hydrodynamic case, when a magnetic field is present the steady solution (50) does satisfy the vanishing of the streaming flow as the distance from the walls tends

to infinity [26]. This means that the streaming motion does not penetrate from the boundary layer into the potential flow. Figure 5 shows the contribution to the tangential velocity $\partial\xi_{1s}/\partial y$ as a function of the y-coordinate at a fixed position within the fringing field ($x = 0.5$) for increasing values of N_ω, with $R_\omega = 10$, $K = 0.8$ and $x_0 = 0.5$. It can be observed that as N_ω increases $\partial\xi_{1s}/\partial y \to 0$ and therefore the steady streaming becomes weaker as the strength of the field grows. This means that the disturbance created by streaming vortices at the extremes of the generator should not affect its performance drastically.

The steady part of the stream function, $\psi_{1s}(x, y) = U_0(dU_0/dx)\xi_{1s}$, is shown in Fig. 6 as a function of the $x-$coordinate for different values of the constant x_0 that modulates the magnetic field gradient. The influence of the fringing region is clearly shown, the largest values of ψ_{1s} occur when the field gradient is more pronounced. This shows that the stronger the magnetic field gradient the more confined the streaming vortices are and the more intense the flow is.

In Fig. 7, the streamlines in the fringing field region are displayed for the cases $x_0 = 0.5$ and $x_0 = 1.5$. Two steady recirculations are observed which extend, accordingly to the value of x_0, across the zone where the magnetic field passes from a uniform value to zero.

5. Concluding remarks

We have explored the zero-mean oscillatory two-dimensional flow of a liquid metal in an alternate MHD generator driven by an imposed harmonic pressure gradient. The finite extension of the applied magnetic field transverse to the electrically insulating duct walls was considered for the analysis of the flow behavior. In the uniform field region, characteristic flows were explored through asymptotic solutions for a small ($R_\omega \ll 1$) and high ($R_\omega \gg 1$) oscillation frequencies and arbitrary Hartmann numbers. For small frequencies, a first order quasi-steady Hartmann flow in phase with the pressure gradient is obtained, while an out of phase contribution is found at $O(R_\omega)$. For high frequencies a solution for the core and boundary layer was obtained. The core solution represent a uniform time periodic flow that lags from the imposed pressure gradient according to the strength of the magnetic field. When the magnetic field is negligible, a purely hydrodynamic flow is obtained and the lag between the core and the pressure gradient is $-\pi/2$. For very strong magnetic field, the lag is negligible and the core follows the pressure gradient oscillation. Out of phase and in phase contributions were also found in the boundary layer, where a purely hydrodynamic (Stokes) boundary layer is obtained for negligible field while a Hartmann layer, oscillating in phase with the pressure gradient, is obtained for strong fields. These results can be conveniently synthesized graphically.

The analysis of the entrance oscillatory flow in the fringing field region at the edges of the MHD generator was carried out for high oscillation frequencies using a perturbation method, assuming the small amplitude of oscillation approximation. From the first order solution, the thickness of the boundary layer was estimated, and it resulted a combination of the Stokes and Hartmann layers, each of which are recovered in the corresponding limits. The second order solution revealed that, superimposed to the primary oscillatory flow, a secondary flow composed by a time periodic motion oscillating with twice the original frequency and a steady streaming contribution exist. A pair of steady streaming vortices emerges in the fringing field region as a consequence of non-linear effects caused by the spatial variation of the magnetic field. The extension and intensity of the vortices grow as the magnetic field gradient increases. Unlike the hydrodynamic case, these vortices do not penetrate into the potential flow but remain confined in the boundary layer and, moreover, their strength decreases as the magnetic field becomes stronger. Although the disturbance created by the steady streaming vortices is not expected to affect the performance of the MHD generator, one could conveniently consider a smooth magnetic field gradient for design purposes.

Acknowledgments

This work was supported by *Centro Mexicano de Innovación en Energía Océano*, CEMIE-Océano No. 249795 SENER-CONACYT and by CONACYT under Project 240785.

Appendix

A.

The constants appearing in Eq. (45) are defined as follows:

$$\kappa_{t1} = \frac{\vartheta_{t1} + \vartheta_{t2}}{\vartheta_{t3}},$$

$$\kappa_{t2} = \frac{\vartheta_{t4} + \vartheta_{t5}}{\vartheta_{t6}},$$

$$\kappa_{t3} = \frac{U_0\left(\alpha' + i\beta'\right)}{\gamma^2\left(\lambda^2 - 8i\alpha\beta - 4\alpha^2 + 4\beta^2\right)},$$

$$\kappa_{t4} = \frac{\vartheta_{t7}}{\gamma^2\lambda(\gamma+\lambda)^2(2\gamma+\lambda)},$$

where

$$\begin{aligned}
\vartheta_{t1} &= 2U_0'\Big[\lambda^4 - \alpha^2\left(7\lambda^2+72\beta^2\right) + 48i\alpha^3\beta + 12\alpha^4 + 7\lambda^2\beta^2 + 12\beta^4 - 2i\alpha\left(7\lambda^2\beta + 24\beta^3\right)\Big],\\
\vartheta_{t2} &= -2\gamma U_0\left(\lambda^2 + 10i\alpha\beta + 5\alpha^2 - 5\beta^2\right)\left(\alpha' + i\beta'\right),\\
\vartheta_{t3} &= \left(\lambda^3 - 4\gamma^2\lambda\right)\left(\lambda^2 - 2i\alpha\beta - \alpha^2 + \beta^2\right)^2,\\
\vartheta_{t4} &= -2U_0'[2\lambda^2 + 4\beta^2 + \alpha\left(-8i\beta + 3y\beta^2 + \lambda^2 y\right) + \alpha^2(-4 - 3iy\beta) - y\alpha^3 + i\lambda^2 y\beta + iy\beta^3],\\
\vartheta_{t5} &= 2U_0\left(\alpha' + i\beta'\right)\left(-2i\beta + \alpha(-2 - 2iy\beta) - y\alpha^2 + y\beta^2 + \lambda^2 y\right)\big),\\
\vartheta_{t6} &= \gamma\left(\lambda^2 - 2i\alpha\beta - \alpha^2 + \beta^2\right)^2\\
\vartheta_{t7} &= 12\alpha^3 U_0' - 12i\beta^3 U_0' + \alpha^2\Big[2U_0'(7\lambda + 18i\beta) - 5U_0\left(\alpha' + i\beta'\right)\Big] + \beta^2\left(-14\lambda U_0' + 5U_0\left(\alpha' + i\beta'\right)\right)\\
&\quad + 2\alpha\Big[2U_0'\left(\lambda^2 + 7i\lambda\beta - 9\beta^2\right) - U_0(2\lambda + 5i\beta)\left(\alpha' + i\beta'\right)\Big] - \lambda^2 U_0\left(\alpha' + i\beta'\right) + 4\lambda\beta i\lambda U_0' + 4\lambda\beta U_0\left(\beta' - i\alpha'\right).
\end{aligned}$$

The constants appearing in Eq. (50) are defined as follows:

$$\begin{aligned}
\kappa_{s1} &= \frac{\lambda_s\left(-2\alpha^2\left(\lambda_s^2 - \beta^2\right) + \alpha^4 + \left(\lambda_s^2 + \beta^2\right)^2\right)^2\vartheta_{s1}}{(\gamma - \lambda_s)^2\alpha^2\left(\gamma\overline{\gamma}\right)^2},\\
\kappa_{s2} &= \frac{\vartheta_{s2}}{(\gamma - \lambda_s)^2},\\
\kappa_{s3} &= \frac{(\lambda_s - 2\alpha)^2(\lambda_s - \alpha + i\beta)^2\vartheta_{s3}}{\alpha^2\left(\gamma\overline{\gamma}\right)^2},\\
\kappa_{s4} &= \frac{\lambda_s(\gamma + \lambda_s)^2\left(\lambda_s^2 - 4\alpha^2\right)^2\vartheta_{s4}}{\left(\gamma\overline{\gamma}\right)^2},\\
\kappa_{s5} &= \frac{\lambda_s\left(\lambda_s^2 - 4\alpha^2\right)^2\left(\lambda_s^2 + 2i\alpha\beta - \alpha^2 + \beta^2\right)^2\vartheta_{s5}}{(\gamma - \lambda_s)^2\left(\gamma\overline{\gamma}\right)^2},\\
\kappa_{s6} &= 4\lambda_s(\gamma + \lambda_s)^2(\lambda_s - 2\alpha)^2(\lambda_s + 2\alpha)^2(\lambda_s + \overline{\gamma})^2(\lambda_s - \alpha + i\beta)^2,
\end{aligned}$$

where

$$\begin{aligned}
\vartheta_{s1} &= 2\lambda_s^2\alpha\beta^4\left(U_0' - yU_0\alpha'\right) - \lambda_s^2 U_0\beta^4\alpha' - 4U_0\alpha^6\left(\alpha' + 2y\beta\beta'\right) - 8\alpha^5\beta\left(\beta\left(U_0' - yU_0\alpha'\right) + 3U_0\beta'\right) + 2U_0\left(\lambda_s^2 - 2\beta^2\right)\beta'\big)\\
&\quad + U_0\alpha^4\left(\alpha'\left(\lambda_s^2 + 24\beta^2\right) + 2y\beta\left(\lambda_s^2 - 4\beta^2\right)\beta'\right) + 2U_0\alpha^2\beta^2\left(\lambda_s^2 y\beta\beta' - 2\alpha'\left(\lambda_s^2 - 3\beta^2\right)\right)\big)\\
&\quad + 2\alpha^3\beta\left(\beta\left(\lambda_s^2 - 4\beta^2\right)\left(U_0' - yU_0\alpha'\right)\right.,\\
\vartheta_{s2} &= (\lambda_s^2 - 4\alpha^2)U_0'\Big[\alpha^6\left(2\beta^2 - 31\lambda_s^2\right) + 12\alpha^8 + \alpha^4\left(27\lambda_s^4 - 9\lambda_s^2\beta^2 - 34\beta^4\right) + \left(\lambda_s^2 + \beta^2\right)^2\left(\lambda_s^4 + \lambda_s^2\beta^2 - 2\beta^4\right)\\
&\quad - \alpha^2\left(9\lambda_s^6 + 20\lambda_s^4\beta^2 + 45\lambda_s^2\beta^4 + 26\beta^6\right)\Big] + U_0\Big[\alpha\Big(20\alpha^8 - \alpha^6\left(41\lambda_s^2 + 108\beta^2\right) + \alpha^4\left(21\lambda_s^4 + \lambda_s^2\beta^2 - 156\beta^4\right)
\end{aligned}$$

$$+\alpha^2\left(\lambda_s^6+58\lambda_s^4\beta^2+13\lambda_s^2\beta^4-36\beta^6\right)-\left(\lambda_s^2+\beta^2\right)\left(\lambda_s^6+22\lambda_s^4\beta^2\right)-\left(\lambda_s^2+\beta^2\right)\left(21\lambda_s^2\beta^4+8\beta^6\right)\Big)\alpha'$$

$$+\beta\Big(100\alpha^8-\lambda_s^2(\lambda_s-\beta)(\lambda_s+\beta)\left(\lambda_s^2+\beta^2\right)^2\alpha^6\left(76\beta^2-107\lambda_s^2\right)-\alpha^4\left(15\lambda_s^4+69\lambda_s^2\beta^2+20\beta^4\right)$$

$$+\alpha^2\left(23\lambda_s^6+66\lambda_s^4\beta^2\right)+\alpha^2(+39\lambda_s^2\beta^4+4\beta^6)\Big)\beta'\Big],$$

$$\vartheta_{s3}=24\alpha^{10}U_0'+\lambda_sU_0\beta^4\alpha'\left(\lambda_s^2+\beta^2\right)^2+2\alpha^9\left(44\lambda_sU_0'-5U_0\alpha'\right)+2\alpha\beta^4\left(\lambda_s^2+\beta^2\right)\left(2U_0\alpha'\left(2\lambda_s^2+\beta^2\right)-\lambda_sU_0'\left(\lambda_s^2+\beta^2\right)\right)$$

$$+\alpha^4\Big(-52\beta^6U_0'-\lambda_s^5U_0\alpha'+6\lambda_s^3\beta^2\left(2\lambda_sU_0'+17U_0\alpha'\right)+2\lambda_s\beta^4\left(68U_0\alpha'-59\lambda_sU_0'\right)-32\lambda_s^4U_0\beta\beta'-44\lambda_s^2U_0\beta^3\beta'$$

$$+10U_0\beta^5\beta'\Big)+2\alpha^2\Big(2\lambda_s^5U_0\beta^2\alpha'+\lambda_s\beta^6\left(11U_0\alpha'[x]-13\lambda_sU_0'\right)-2\beta^8U_0'+\lambda_s^3\beta^4\left(17U_0\alpha'-9\lambda_sU_0'\right)+\lambda_s^2U_0\beta^5\beta'$$

$$-U_0\beta^7\beta'\Big)+2\alpha^3\beta\Big(\beta\left(U_0'\left(\lambda_s^5-32\lambda_s^3\beta^2-31\lambda_s\beta^4\right)+U_0\alpha'\left(16\lambda_s^4+47\lambda_s^2\beta^2+9\beta^4\right)\right)-2\lambda_sU_0(\lambda_s^4+2\lambda_s^2\beta^2$$

$$-3\beta^4)\beta'\Big)+\alpha^8\Big(2U_0'\left(63\lambda_s^2+2\beta^2\right)-U_0\left(33\lambda_s\alpha'+50\beta\beta'\right)\Big)+2\alpha^7\Big(11\lambda_sU_0'\left(4\lambda_s^2+\beta^2\right)-U_074\lambda_s\beta\beta'$$

$$+U_03\alpha'\left(9\beta^2-7\lambda_s^2\right)\Big)+2\alpha^6\Big(U_0'\left(15\lambda_s^4+17\lambda_s^2\beta^2-34\beta^4\right)+U_0\left(\lambda_s\alpha'\Big(73\beta^2-13\lambda_s^2\Big)-\beta\left(87\lambda_s^2+19\beta^2\right)\beta'\right)\Big)$$

$$+2\alpha^5\Big(U_0'2\lambda_s^5+\left(14\lambda_s^3\beta^2-63\lambda_s\beta^4\right)U_0'+U_0\alpha'\left(-4\lambda_s^4+84\lambda_s^2\beta^2+39\beta^4\right)-U_04\beta\left(13\lambda_s^3+9\lambda_s\beta^2\right)\beta'\Big),$$

$$\vartheta_{s4}=-y\alpha^6U_0'+\alpha^5\left(U_0'(-4+2iy\beta)+yU_0\left(\alpha'-i\beta'\right)\right)+\alpha^2\Big[\beta\Big(U_0'\left(4i\lambda_s^2+\beta\left(2\lambda_s^2y+\beta(y\beta+8i)\right)\right)+U_0\alpha'(2\beta(6-iy\beta)$$

$$-i\lambda_s^2y)\Big)-U_0\beta'\left(-2i\lambda_s^2+\lambda_s^2y\beta+2y\beta^3\right)\Big]+\beta^2\Big[\beta\Big(U_0'\left(4i\lambda_s^2+\beta\left(\lambda_s^2y+\beta(y\beta+6i)\right)\right)-iU_0\alpha'\left(\lambda_s^2y+\beta(y\beta+2i)\right)\Big)$$

$$-U_0\beta'\left(2i\lambda_s^2+\beta\left(\lambda_s^2y+\beta(y\beta+4i)\right)\right)\Big]+\alpha\beta\Big(\lambda_s^2\beta\left(2U_0'-yU_0\left(\alpha'-i\beta'\right)\right)+2iy\beta^4U_0'-4i\lambda_s^2U_0\alpha'$$

$$+\beta^3\left(-8U_0'+yU_0\left(\alpha'-i\beta'\right)\right)+4U_0\beta^2\left(\beta'-i\alpha'\right)\Big)+\alpha^4\Big(U_0'\left(\lambda_s^2y+\beta(-y\beta+2i)\right)+U_0\left(\alpha'(2-iy\beta)-\beta'(y\beta+4i)\right)\Big)$$

$$+\alpha^3\Big(U_0\left(\alpha'\left(-\lambda_s^2y+2\beta(y\beta+2i)\right)+i\beta'\left(4i\beta-2y\beta^2+\lambda_s^2y\right)\right)+2U_0'\left(\lambda_s^2-6\beta^2+2iy\beta^3\right)\Big),$$

$$\vartheta_{s5}=-y\alpha^6U_0'+\alpha^5(U_0'(-4-2iy\beta)+yU_0(\alpha'+i\beta'))+\alpha^2\Big(\beta(U_0'(\beta(2\lambda_s^2y+\beta(y\beta-8i))-4i\lambda_s^2)$$

$$+U_0\alpha'(2\beta(6+iy\beta)+i\lambda_s^2y)\Big)-U_0\beta'\left(2i\lambda_s^2+\lambda_s^2y\beta+2y\beta^3\right)\Big)+\beta^2\Big(\beta\left(U_0'\left(\beta\left(\lambda_s^2y+\beta(y\beta-6i)\right)-4i\lambda_s^2\right)\right.$$

$$\left.+U_0\alpha'\left(\beta(2+iy\beta)+i\lambda_s^2y\right)\right)-U_0\beta'\left(\beta\left(\lambda_s^2y+\beta(y\beta-4i)\right)-2i\lambda_s^2\right)\Big)+\alpha\beta\Big(\lambda_s^2\beta\left(2U_0'-yU_0\left(\alpha'+i\beta'\right)\right)$$

$$+4i\lambda_s^2U_0\alpha'-2iy\beta^4U_0'+\beta^3\left(-8U_0'+yU_0\left(\alpha'+i\beta'\right)\right)+4U_0\beta^2\left(\beta'+i\alpha'\right)\Big)+\alpha^4\Big(U_0'\left(\lambda_s^2y-\beta(y\beta+2i)\right)$$

$$+U_0\left(\alpha'(2+iy\beta)+\beta'(-y\beta+4i)\right)\Big)+\alpha^3\Big(2U_0'\left(\lambda_s^2-6\beta^2-2iy\beta^3\right)-U_0\alpha'\left(4i\beta(x)-2y\beta(x)^2+\lambda_s^2y\right)$$

$$+U_0\beta'(-4\beta(x)+2iy\beta(x)^2-i\lambda_s^2y)\Big).$$

1. A. Alemany, A. Krauze, and M. A. Radi, *Energy Proc.* **6** (2011) 92-100.
2. S. M. H. Mirhoseini, A. Alemany, *Magnetohydrodynamics* **51** (2015) 519-530
3. L. Hu, H. Kobayashi, Y. Okuno, Performance of a liquid metal MHD power generation system for various external forces *Proc. 12th Int. Energy Conv. Eng. Conf.*, Cleveland, OH, July 28-30, (2014), AIAA 2014-3558.
4. B. Liu, J. Li, Y. Peng, L. Zhao, R. Li, Q. Xia, C. Sha, Performance Study of Magnetohydrodynamic Generator for Wave Energy, *Proc. 19th ISOPE Conf.* Busan, Korea, June 15-20 (2014) 545.
5. V. R. Malghan, *Energy Conv. Mgmt.* **37** (1996) 569-590.
6. G.W. Swift, *J. Acoust. Soc. Am.* **83** (1988) 350-361.
7. A.A. Castrejón-Pita, G. Huelsz, *Appl. Phys. Lett.*, **90**, (2007) 174110.
8. C. Vogin and A. Alemany, *Eur. J. Mech.-B/Fluids*, **26** (2007) 479-493.
9. D. A. Altshuller, R. A. Koslover, Optimal Control of the Magnetohydrodynamic Ocean Wave Energy Converter: Theory. *Proc. IEEE 2005 Int. Conf. Phys. Control*, Saint Petersburg, Russia, Aug. 24-26 (2005) 126.
10. L. Zhao, Y. Peng, C. Sha, R. Li, Y. Xu, B. Liu and J. Li, Effect of Liquid Metal Characteristics on Performance of LMMHD Wave Energy Conversion System *Proc. 24th ISOPE Conf.* Osaka, Japan, June 21-26, (2009) 308.
11. B. Liu, Y. Peng, L. Zhao, J. Li, R. Li, Y. Xu, C. Sha, Hydrodynamic modelling of heaving buoy wave energy conversion system with liquid metal magnetohydrodynamic generator, *Proc. 21st ISOPE Conf.*, Maui, Hawaii, USA, June 19-24, (2011) 695.
12. U. Müller, L. Bülher, *Magnetofluyddynamics in channels and containers*, (Springer, 2001).
13. J. A. Rizzo-Sierra, O. I. López-Hernández, *Rev. Mex. de Fís.* **62** (2016) 369-380.
14. R. Moreau, S. Smolentsev and S. Cuevas, *PMC Physics B* **3** (2010) 3.
15. T. Zhou, H. Chen and Z. Yang, *Fusion Eng. Design*, **86** (2011) 2352-2357.
16. H. K. Moffatt and J. Toomre, *J Fluid Mech.* **30** (1967) 65-82.
17. G. Ibáñez, S. Cuevas and M. López de Haro, *Energy Conv. & Management*, **43** (2002) 350-361.
18. G. Leal, *Advanced transport phenomena*, Cambridge University Press, 2007.
19. H. Perales, *Numerical study of oscillatroy flows in ducts*, Doctoral thesis, Facultad de Ciencias, Universidad Autónoma del Estado de Morelos, Mexico, April 2003 (in Spanish).
20. A. Yakhot and L. Grinberg, *Phys. Fluids* **15** (2003) 2081-2083.
21. H. Schlichting, *Boundary layer theory*, 7th ed. McGraw-Hill, New York, (1979) pp.428-432.
22. N. Riley, *Ann. Rev. Fluid Mech* **33** (2001) 43-65.
23. I. S. Goldberg, Z. Zhang and M. Tran, *Phys. Fluids* **11** (1999) 2957-2962.
24. A. Gopinath, *Q. J. Mech. Appl. Math.* **47** (1994) 461-480.
25. J. T. Stuart *J. Fluid Mech.* **24** (1966) 673-687.
26. S. Cuevas and E. Ramos. *Phys. Fluids* **9** (1997) 1430-1434.
27. A. Sterl. *J. Fluid Mech.* **216** (1990) 161-191.